2016 IEEE International Conference on Advanced Intelligent Mechatronics (AIM)
Banff, Alberta, Canada, July 12–15, 2016

Real-time Needle Shape Prediction in Soft-Tissue based on Image Segmentation and Particle Filtering

Jay Carriere[1], Carlos Rossa[1], Ronald Sloboda[2], Nawaid Usmani[2], Mahdi Tavakoli[1]

***Abstract*— Prostate brachytherapy is a current technique used to treat cancerous tissue in the prostate by permanently implanting radioactive seeds through the use of long flexible needles. This paper proposes a real-time method to predict the shape of a flexible needle inserted into soft tissue using axial Transrectal Ultrasound (TRUS) image segmentation and a non-holonomic bicycle model informed via particle filter. The needle location is tracked in TRUS images to capture the needle shape up to a specified depth. Through the use of a particle filter the noisy tracked needle shape is used to update the parameters of a kinematic bicycle model in a robust manner to predict the shape of the entire needle after it is fully inserted. The method is verified in both ex-vivo beef phantom tissue and in-vivo clinical images, yielding an average tip prediction error of less that 0.5 mm in both the ex-vivo and in-vivo image sets with a peak processing time of less than 9.5 ms per image frame.**

I. INTRODUCTION

Prostate brachytherapy is a percutaneous minimally-invasive surgery whereby long flexible needles containing radioactive seeds are inserted into the prostate. Prostate brachytherapy is effective and well-tolerated, with the efficacy and side effect profile primarily determined by the inaccuracy with which the seeds are placed with regard to their pre-planned target locations. Current clinical setups for prostate brachytherapy, diagrammed in Fig 1, consist of a guide template, which has a grid of holes through which the needle is inserted, a transrectal ultrasound (TRUS) probe, and the brachytherapy needle. A clinician uses a guide template to position the needle in line with a preplanned target location and ultrasound imaging in the axial plane, showing a cross section of the needle, is used to verify the placement of the needle near the target location. The beveled edge of the needle meant to facilitate tissue cutting will also cause the needle to deflect away from the desired target location, thus causing seed placement errors.

Ultrasound image based needle segmentation and tracking has been approached in both 2D axial and sagittal image slices, taken along the length of the needle as it is inserted, as well as in 3D volumes. This paper will focus on tracking the needle position in individual 2D axial slices, as 3D ultrasound technology is still quite expensive and presents additional computational challenges. Saggital image needle segemtation has the disadvantage that a substantial portion of the needle needs to be captured in the image plane in order for segmentation to work. From our group [1] used RANSAC to robustly detect the needle from a complete set of axial images, and to display the full 3D shape of the needle in an off-line method. [2] and [3] outline a kinematic model of needle motion based on the well-known bicycle model. In this paper, we build on these methods using particle filtering to solve for the parameters of the bicycle model in the presence of measurement uncertainty in the ultrasound images. Particle filters are widely used in signal processing [4] and image processing [5] [6] to fit parameters and characterize noise in model based systems.

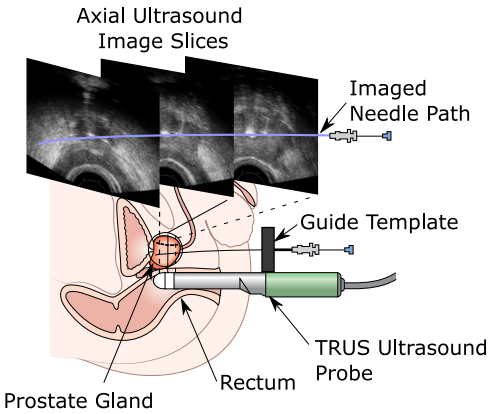

Fig. 1: Standard brachytherapy setup with TRUS probe and template. Figure courtesy of Cancer Research UK/Wikimedia Commons.

The primary goal of this paper is to combine a kinematic model of the brachytherapy needle with an image processing routine that tracks the needle tip during insertion to build a robust needle shape estimation system. Our proposed algorithm predicts the shape of the entire needle based on the observation of only a portion of the needle with the assumption that the needle shape can be described in a single 2D plane. Using the needle shape information a clinician will then be able to determine if the needle tip position, and subsequently the deposited seed position, will be placed at a satisfactory location. This allows corrective action to be taken without withdrawing and fully reinserting the needle and thereby reducing tissue damage. Additionally, by predicting

This work was supported by the Natural Sciences and Engineering Research Council (NSERC) of Canada under grant CHRP 446520, the Canadian Institutes of Health Research (CIHR) under grant CPG 127768, and by the Alberta Innovates - Health Solutions (AIHS) under grant CRIO 201201232.

[1]Jay Carriere, Carlos Rossa, and Mahdi Tavakoli (Corresponding Author) are with the Department of Electrical and Computer Engineering, University of Alberta, AB, Canada T6G 2V4. E-mail: jtcarrie@ualberta.ca; rossa@ualberta.ca; mahdi.tavakoli@ualberta.ca.

[2]Ronald Sloboda and Nawaid Usmani are with the Cross Cancer Institute and the Department of Oncology, University of Alberta, Edmonton, AB, Canada T6G 1Z2. E-mail: ron.sloboda@albertahealthservices.ca; nawaid.usmani@albertahealthservices.ca.

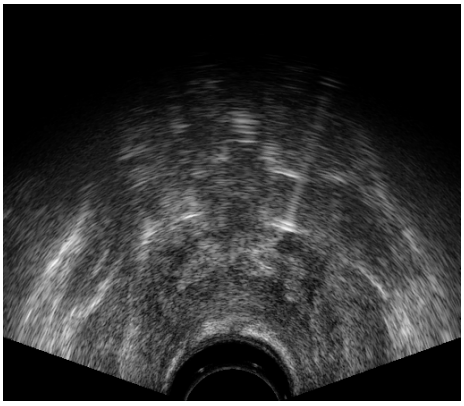

Fig. 2: Original patient image

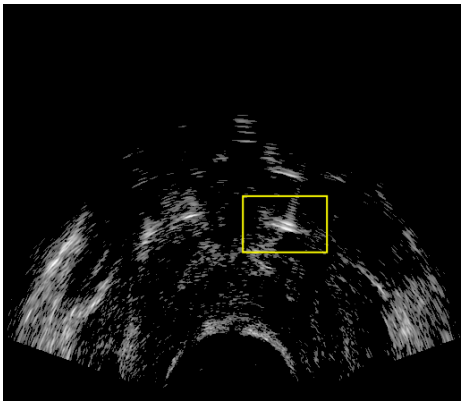

Fig. 3: Variance image with selected template patch

the needle shape and tip position, the TRUS ultrasound probe can remain stationary after a pre-defined stopping point, thus minimizing the effect of TRUS probe movement on needle shape and final tip displacement. In the future, this needle tracking and estimation routine will be used to inform a needle steering control system.

For tracking and prediction the position of the needle cross-section is segmented out of each of the 2D axial slices, taken normal to the insertion direction of the of the needle. The tracked needle cross section and the distance between consecutive axial slices is incorporated by a particle filter to update the parameters of a non-holonomic kinematic bicycle model for each image slice. As the kinematic parameters are being updated the predicted needle shape is used to augment the needle tracking routine by determining a likely location for the position of the needle cross-section in the current and future axial slices. The error in the predicted needle cross section location is the primary method through which the particle filter updates the parameters of the kinematic model. The kinematic model parameters are updated until a pre-specified insertion depth and then the kinematic model is used to predict the final shape of the fully inserted needle.

This paper will be organized as follows, Section II will go over the needle segmentation and tracking routine. Section III will cover the kinematic bicycle model of a needle, which will be used for needle shape prediction. Section IV contains the implementation of the particle filter that is used to update parameters of the kinematic model of the needle in real time. Section V gives the experimental setup to be used for phantom tissue and clinical* images, and outlines the results of the algorithm.

II. IMAGE PROCESSING

During the clinical and experimental procedures, ultrasound images are taken normal to the needle's insertion direction; see Fig 1. The method chosen to process the images is based on the Lucas-Kanade tracking method [7]. Using the results of [8] and [9], an active tracking method was devised in order to incorporate both the current imaging data as well as information from the model prediction.

*Approval for study granted from Alberta Cancer Research Ethics Committee under reference 25837

The clinical axial images, Fig. 2, are taken exactly 5 mm apart and the entire image set was captured after the needle was fully inserted into the prostate. For the experimental images, the probe was translated along the direction of needle insertion in order to capture the needle tip cross section at 0.5 mm intervals. Given the assumptions in [2] that the needle path perfectly follows the tip position as it is inserted, the two imaging cases return the same information about needle shape or equivalently needle tip location.

Our algorithm divides the image processing into a pre-processing phase and a tracking phase. In the pre-processing phase, the entire image is enhanced in order to increase the signal-to-noise ratio. The desired signal is the brightness of the image pixels corresponding to the needle cross section and the noise is the brightness of the background pixels representing the surrounding tissue. After pre-processing the filtered image goes on to the tracking phase. The tracking phase uses a template patch of pixels around the needle cross section in the current image slice to determine the location of the needle cross section in the subsequent image slice. The region of interest that is searched to find the needle cross section is informed by the predicted location of the needle to limit the template matching search area.

Each image I_k is captured at a discrete time step k. Here we will define the pixel brightness, or intensity, to be $I_k(px, py)$ at each point px, py in the image. The pre-processing stage calculates the variance image V_k in order to increase the brightness of the needle cross section pixels with respect to the average background pixel brightness. The formula for intensity of the variance image pixels $V_k(px, py)$ is given as follows,

$$V_k(px, py) = \left(I_k(px, py) - \overline{I_k}\right)^2 \tag{1}$$

where $\overline{I_k}$ is the average pixel intensity of the image. The intensity of the variance image was normalized to be with 0 to 1 in our implementation by dividing each of the variance pixels $V_k(px, py)$ by largest value of $V_k(px, py)$ in the variance image. The result of this operation on Fig 2 is shown in Fig 3.

The next phase of the image processing routine is to localize the needle in each variance image. The center point of the needle cross section will be used as the needle location

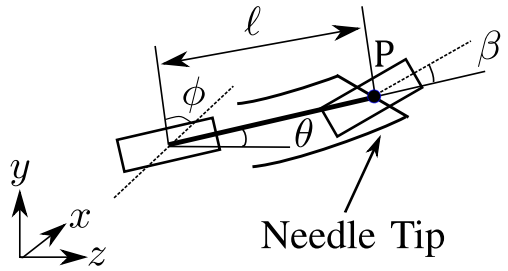

Fig. 4: Nonholonmic bicycle model of needle motion in 3D

in the axial image slice and is referred to as I_{ck}. For the first axial image slice, at time step k_0, a user will manually select a point I_{c0} that corresponds to center of the needle cross section in that slice. A template patch of pixels I_{t0} is created around the needle cross section with height h and width w; Fig 3. This template I_t is compared to the variance image of the subsequent axial slice using normalized cross correlation (NCC) [9]. The best match, with respect to NCC value, is used to localize the center of the needle cross section, I_{ck}, in that image. Due to the variation in needle cross section intensity and appearance across all of the axial slices the template patch I_t is updated for each frame and consists of the values of the variance image around the center of the needle cross section.

In order to speed up template matching we restrict the NCC calculations to be within a region of interest of height $2h$ and width $2w$. Nominally the region of interest is centred around the kinematic model prediction of the needle cross section location. For the first 10 mm of the needle insertion, however, the region of interest is centred around the previous needle cross section center I_{ck-1}. After the needle inserted past the 10 mm depth the mean value from the particle filter is used in the kinematic bicycle model to predict the needle shape. The predicted location of the needle cross section in the current axial slice is used as the center of the region of interest. Note that the position of I_{ck} in px, py is scaled using a predetermined $\frac{pixel}{mm}$ ratio for the x and y axis before being input into the particle filtering routine, to be described in the Sec IV.

III. KINEMATIC MODEL

The model to be used in this paper is the kinematic bicycle model presented in the context of needle modleing in [2] and [3]. This model approximates the motion of a needle cutting through tissue as a constant curvature motion that is dependent on the angle of the bicycles' front wheel β and the distance ℓ between the two bicycle wheels, see Fig 4. For use in this paper, the parameters of the bicycle model will be initialized and updated as described in Section IV. Using the state space formulation of the kinematic bicycle model, the states of the system are given by $X_{k|k} = [x, y, z, \theta, \phi]^T$, where x, y and z are the coordinates of the needle tip at time step k, θ is the angle of the needle tip at time k, and ϕ is the rotation angle about the z axis for the plane that contains the needle deflection. The value of ϕ will be considered to be constant throughout the insertion procedure. The control inputs to the state space system are given by $U_{k|k} = [\alpha, \beta]^T$, where α is the needle insertion distance along the z direction per time step. We consider the needle bevel angle β to be alternating between a positive and negative constant, corresponding to a rotation of the needle bevel of 180° about the z axis. The value of β is the rate of change of needle tip angle θ per time step.

The state-space equation of the non-holonomic bicycle model in 3D is given as

$$X_{k+1|k} = I_5 X_{k|k} + \begin{bmatrix} \sin(\theta)\sin(\phi) & 0 \\ \sin(\theta)\cos(\phi) & 0 \\ \cos(\theta) & 0 \\ 0 & 1 \\ 0 & 0 \end{bmatrix} U_{k|k} \quad (2)$$

where I_5 is the five-by-five identity matrix. The values of ℓ and β can be used to determine a radius of curvature R about a center of motion defined in general as x_c, y_c, z_c in 3D space, where $R = \frac{\ell}{\sin(\beta)}$. Given the value of ϕ, we are able to define a new 2D coordinate system u, v, Fig 5, that will be used to represent the in-plane motion of the needle tip. Here u will be the coordinate that represents the in-plane deflection of the needle shape and v will be parallel to the insertion direction of the needle, making it equivalent to z in the general coordinate system.

The particle filter, outlined in Sec IV, requires that the needle shape from the bicycle model be simulated many times per frame. In order to reduce the state-space model into a form that is more computationally efficient we derive a piece-wise solution to the state space equation. This piece-wise solution allows us to predict the needle shape based on the parameters of the bicycle model. The needle shape is given by tracing the path of the needle tip point P as the needle is inserted into tissue. The piece-wise nature of the solution is used to allow simulation of the needle path for an arbitrary number of rotations. The equation of motion of the needle tip point P is given by

$$u = u_c(i) \pm \sqrt{R^2 - (v - v_c(i))^2} \quad (3)$$

in the u, v coordinate system. Where the values of $u_c(i)$ and $v_c(i)$ are the center of rotation for the circular needle motion. The value i is used to allow for multiple centers of rotation that correspond to rotating the needle by 180° about the v, or equivalently z axis. The values of $u_c(i)$ and $v_c(i)$ can be found through the following formula

$$\begin{aligned} u_c(i) &= \pm R \times \cos(\theta) + u_{turn}(i) \\ v_c(i) &= \pm R \times \sin(\theta) + v_{turn}(i) \end{aligned} \quad (4)$$

where $u_{turn}(i)$ and $v_{turn}(i)$ are the values of u and v at the moment when the needle is rotated 180°. For $u_c(0)$ and $v_c(0)$ corresponding to center of rotation at needle insertion, and before rotation, the values of $u_{turn}(0) = 0$ and $v_{turn}(0) = 0$. Note that only a singular value of $\pm R$ is used in the formulation, i.e. either a positive or negative R, and that this corresponds to an convex or concave curvature of the needle

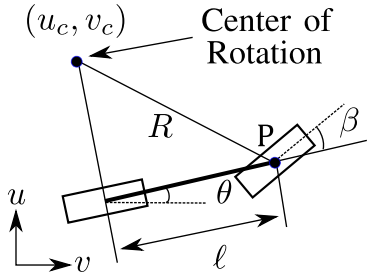

Fig. 5: Needle Motion around Center of Rotation in u, v Plane

which will be solved for in the subsection IV. The position of the needle tip in the x, y, z coordinate system is

$$\begin{aligned} x &= \cos(\phi) \times u \\ y &= \sin(\phi) \times v \\ z &= v \end{aligned} \tag{5}$$

Using this equation we can have then simplified solving for all of the model parameters into solving for the center of rotation for each time step k, which will be done through the use of the previous described image based needle tracking routine and the particle filter, as will be described in the next section.

IV. PARTICLE FILTERING

A particle filter will be used to solve for the model parameters in Sec III. Given the low signal-to-noise ratio inherent in ultrasound imaging, primarily due to poor spatial resolution, the data returned from the image processing algorithm (see Sec II) contains significant noise in the measured values of x and y in each image plane. This noise, or jitter, affects the ability to predict the values of β and θ in the state-space bicycle model and has a large impact on the predicted needle shape. The particle filter uses the piece-wise linear solution of the bicycle model to compare multiple predictions of the needle shape to noisy observations of the needle shape from the image processing routine. The mean value of all of the particle filter predictions is then used to predict the entire shape of the needle at each time step k.

The goal of our estimator is to find the parameters of the model before needle rotation at a specified depth D in the z axis (or equivalently the v axis). From (5), it is clear that once we have the value of ϕ, which we solve for using principal component analysis, we are able to formulate a method to fit those parameters on the 2D plane (u, v). We will define the first point the needle passes through as the origin of the coordinate system for the (u, v) plane, and therefore $u_0 = 0$ and $v_0 = 0$. Given that the depth of needle rotation is known, we are able to use (3) and (4) to formulate the following stochastic model of motion for the path of the needle

$$u = u_c(0) \pm \sqrt{R^2 - (v - v_c(0))^2} \tag{6}$$

where

$$\begin{aligned} R &= \sqrt{(u_c(0)^2 + v_c(0)^2)} + \omega_1 \\ \theta_0 &= \tan^{-1}\left(\frac{v_c(0)}{u_c(0)}\right) + \omega_2 \\ \omega_1 &= \mathcal{N}(0, \sigma_1) \\ \omega_2 &= \mathcal{N}(0, \sigma_2) \end{aligned} \tag{7}$$

The values of u and v describe the motion of the needle tip point P in the (u, v) plane. Note that $v \leq D$ is the depth of needle rotation, R is the center of circular motion of the needle, θ_0 is the initial value of θ when the needle is first inserted and ω_1 and ω_2 are Gaussian noise with zero mean and standard deviations σ_1 and σ_2 respectively.

The idea behind particle filtering is to use a large number of particles, n, in order to estimate the probability density function of a noise source. A weight is applied to each of the particles $w(n)$ in order to estimate the output of a function at a time k in the presence of noise. Thus here we used particle filtering to find the values of R and θ_0 based on the noisy observations along the needle path at time k. The mean values of R and θ_0 for all of the particles are used to perform needle path prediction.

As before, k is defined as the time that an image is taken and we will consider all points k_0, the first image in our set, to k_D, the point at time in which the needle is rotated. The particle filter is updated with every image that is processed (refer to Sec II) which defines a nominal sample time of 20 Hz. Given that the goal of the filtering is to determine the parameters for the needle shape we allow the needle to be inserted by 10 mm, denoted by time k_{10mm} before updating the particle weights so that some form of curvature can be detected. This 10 mm section of points also allows for the value of ϕ to be calculated through PCA so that the all of the observed points in (x, y, z) can be transformed into points p in (u, v). The implementation of our particle filter is as follows

1) Initialize n particles randomly with each particle containing a pair of values $R(n)$ and $\theta_0(n)$. A Gaussian random distribution for the particles shall be used where $R(n) \sim \mathcal{N}(\mu_R, \sigma_R)$ and $\theta_0(n) \sim \mathcal{N}(\mu_{\theta_0}, \sigma_{\theta_0})$, for user defined values of μ_R, σ_R, μ_{θ_0}, and σ_{θ_0}
2) At time step k_{10mm}, choose p equidistant points, with respect to their insertion depth v, that are in the set $\{k_0 : k_{10mm}\}$
3) For each of the n particles determine the predicted value of u, denoted by $\hat{u}$, for the corresponding depth v for all of the points p
4) For each particle n determine the L^1 normed distance between the predicted value and the actual value, $L^1(u) = |u - \hat{u}|$
5) Find the values of $R(n)$ and $\theta_0(n)$ that have the minimum L^1 norm for each point p
6) Take the mean value of those minimum $\overline{R(p)}$ and $\overline{\theta_0(p)}$

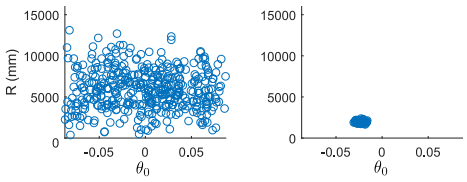

Fig. 6: Inital distribution of R and θ_0 particles and particle convergence after 5 iterations

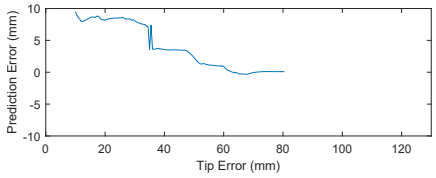

Fig. 7: Decreasing tip prediction error with respect to depth of prediction

7) Using a gain factor γ, update all other particles

$$R(n) = R(n) - \gamma(R(n) - \overline{R(p)})$$
$$\theta_0(n) = \theta_0(n) - \gamma(\theta_0(n) - \overline{\theta_0(p)})$$

8) Calculate the mean and standard deviation of $R(n)$ and $\theta_0(n)$,these are the new values of values of μ_R, σ_R, μ_{θ_0}, and σ_{θ_0}
9) Remove c particles and replace them with c new particles distributed according to the new mean and standard deviation of $R(n)$ and $\theta_0(n)$
10) Take the data from the next step k when it is available and from the set $\{k_0 : k\}$ choose p equidistant points and return to line 3, if $k = k_D$ then terminate returning the mean values, μ_R and μ_{θ_0}

For both the experimental and clinical image sets the values of $n = 500$, $p = 5$, and $c = 3$ were used. The Gaussian distributions for the intial randomization of the particles were chosen to be $R(n) \sim \mathcal{N}(1500, 600)$ and $\theta_0(n) \sim \mathcal{N}(0, 5)$. For this algorithm, we have based our weighting updating methodology on the work of [6] such that we avoid calculating the a priori and a posteriori probability distributions of ω_1 and ω_2 in order to update the particle weights. Instead, we modify the distributions of $R(n) \sim \mathcal{N}(\mu_R, \sigma_R)$ and $\theta_0(n) \sim \mathcal{N}(\mu_{\theta_0}, \sigma_{\theta_0})$ directly from needle shape observation. One of the particular advantages to this method is that by calculating the means, μ_R and μ_{θ_0}, and standard deviations, σ_R and σ_{θ_0}, of our particle set we can evaluate a confidence in our prediction in that the smaller the standard deviation the closer to an ideal value the mean is. Figure 6 shows the convergence of the filter particles at 5 iterations after k_{10mm}, Fig 7 shows the decreasing error of the tip prediction as the filter is iterated from k_{10mm} to the rotation depth $k_D = 80mm$.

V. RESULTS

The ultrasound used for phantom tissue was an Ultrasonix Touch with a 4DL14-5/38 Linear 4D transducer (Ultrasonix Corp, Richmond, BC, Canada). The clinical ultrasound used for the intra-procedure scans is a Sonoline Adara TRUS scanner with an Endo PII probe (Siemens Medical Solutions USA

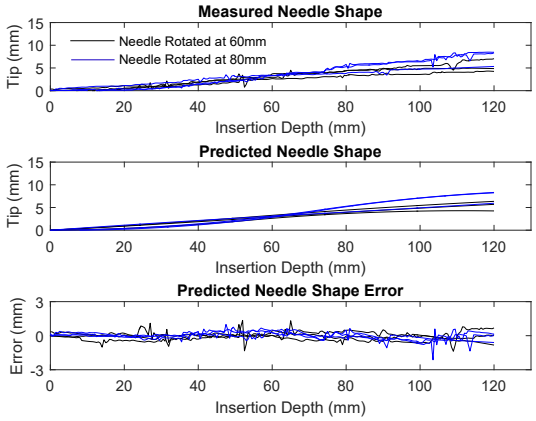

Fig. 8: Needle Shape Prediction vs Acutal Needle Shape for Needle Rotated at 60 mm in Beef Phantom

Inc., Malvern, PA, USA). For both the clinical procedure and the phantom tissue insertions the needles used were 18-gauge 200 mm prostate seeding needles. (Eckert & Zielger BEBIG GmbH, Berlin, Germany).

The ex-vivo tissue phantom was created using beef chuck encased in gelatin. Beef was used to create a non-homogeneous tissue phantom that more closely represents the in-vivo human tissue in both mechanical properties as well as ultrasound imaging characteristics.

The first set of results corresponds to the validation of the particle filtering routine and model after a pre-defined rotation depth (which was not captured in the clinical data) to this end, the needle was inserted into the phantom tissue and rotated at a specified depth. Fig 8 shows the measured needle points and needle shape prediction for 6 needles, which were rotated at a depths of 60 mm and 80 mm.

The second set of results corresponds to the validation of the image processing routine along with particle filtering in clinical data. 6 insertions were used to test that the image processing in particular was successful in tracking the needle position in TRUS images as well as to test the ability for the model to perform successful prediction in real human tissue. The same number of particles and noise parameters for particle initialization was used for both set of results. Being as there was no rotation in the clinical data set the first 35 mm on insertion data was used to predict the entire needle shape.

Two metrics were used to compare the accuracy of the prediction. The first metric was tip error, the difference between the final predicted tip displacement $\hat{u}$ and the measured tip displacement in u, where $\text{TipError} = |u - \hat{u}|$. The second metric to evaluate the shape prediction accuracy is the shape error that compares the absolute areas of the measured and predicted needle shapes in mm^2. The shape error is calculated using the following formula

$$\text{ShapeError} = \int |u - \hat{u}| dv \tag{8}$$

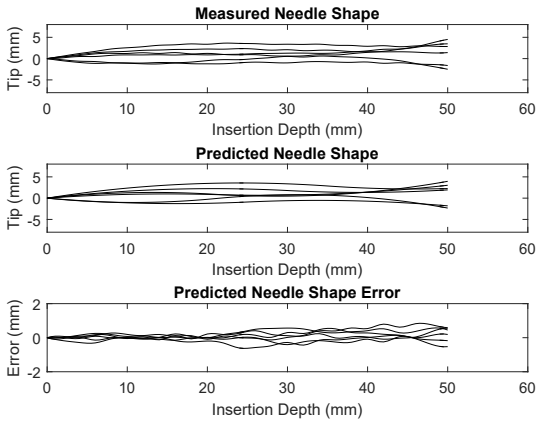

Fig. 9: Needle Shape Prediction vs Acutal Needle Shape for Clincal Image Dataset

TABLE I: Needle Path Prediction Accuracy

Data Set	Tip Prediction Error (mm)	Shape Prediction Error (mm^2)
Beef D60	0.497 ± 0.38	105.0 ± 15.1
Beef D80	0.125 ± 0.02	18.4 ± 5.0
Patient Data	0.44 ± 0.15	19.1 ± 9.6

Using our two metrics of prediction accuracy, in Table I we can see that the more axial image information the particle filter incorporates, corresponding to a larger rotation depth, the more accurate the needle shape prediction. The needle shape errors in the clinical data show that the kinematic model and particle filtering routine work as well on real human tissue as they do on phantom tissue.

The image processing and prediction routines were both coded in Matlab 2015b (The Mathworks Inc, Natwick, MA, USA) and ran on a single core of a Intel Core i7-3930K running at 3.20 GHz (Intel Corporation, Santa Clara, CA, USA). The values of Table II show that the image segmentation and particle filter update routines run in real-time in both the ex-vivo and in-vivo datasets. The peak total processing time, which corresponded to clinical image set, was 9.5 ms. This peak value is well under the 50 ms total time available for image processing and particle filtering, corresponding to the 20 Hz image update frequency. As can be seen from the combined results, our proposed image guided particle filtering routine was able to successfully predict needle shape of a needle inserted into either phantom or ex-vivo tissue in real-time.

TABLE II: Image segmentation and particle filtering update time

Data Set	Image Processing Time (ms/frame)	Particle Filter Update Time (ms/frame)	Total Time (ms/frame)
Beef D60	3.1 ± 0.2	2.8 ± 0.3	5.9 ± 0.4
Beef D80	3.1 ± 0.2	2.6 ± 0.4	5.7 ± 0.4
Patient Data	4.1 ± 0.3	2.4 ± 0.3	6.5 ± 0.3

VI. CONCLUSION

In this paper, we have shown that combining a needle-segmentation routine with a kinematic bicycle model allows for the entire needle shape prediction based on the only on the observation of a portion of the needle as it is inserted. This routine works equally well on ex-vivo beef based phantom tissue and in-vivo clinical images. Normalized cross correlation is used in a template matching route to capture needle position information in axial image slices. This needle position information is input into a particle filtering routine in order to extract the parameters needed to predict the needle shape with a kinematic bicycle model. Both the final needle tip position and needle shape are compared with the measured needle shape to validate the prediction. In general the needle tip position can be predicted with an average error of less than 0.5 mm in both phantom and ex-vivo tissue. This needle shape prediction is also used on-line to augment the needle segmentation process by defining the center of a region of interest for the template matching routine. In future this work will be used to inform a needle steering control routine in order to reduce or remove the needle tip deflection at a desired depth or to inform a surgeon during the brachytherapy procedure about the final shape of the needle before it is fully inserted.

REFERENCES

[1] M. Waine, C. Rossa, R. Sloboda, N. Usmani, and M. Tavakoli, "3D shape visualization of curved needles in tissue from 2D ultrasound images using ransac," in *Robotics and Automation (ICRA), 2015 IEEE International Conference on*, May 2015, pp. 4723–4728.

[2] R. J. Webster, J. S. Kim, N. J. Cowan, G. S. Chirikjian, and A. M. Okamura, "Nonholonomic modeling of needle steering," *The International Journal of Robotics Research*, vol. 25, no. 5-6, pp. 509–525, 2006.

[3] V. Kallem and N. Cowan, "Image guidance of flexible tip-steerable needles," *Robotics, IEEE Transactions on*, vol. 25, no. 1, pp. 191–196, Feb 2009.

[4] M. S. Arulampalam, S. Maskell, N. Gordon, and T. Clapp, "A tutorial on particle filters for online nonlinear/non-Gaussian bayesian tracking," *IEEE Transactions on Signal Processing*, vol. 50, no. 2, pp. 174–188, Feb 2002.

[5] N. Zheng and J. Xue, *Statistical Learning and Pattern Analysis for Image and Video Processing*. London: Springer London, 2009, ch. Probabilistic Data Fusion for Robust Visual Tracking, pp. 245–285.

[6] M. D. Breitenstein, F. Reichlin, B. Leibe, E. Koller-Meier, and L. V. Gool, "Robust tracking-by-detection using a detector confidence particle filter," in *Computer Vision, 2009 IEEE 12th International Conference on*, Sept 2009, pp. 1515–1522.

[7] B. D. Lucas and T. Kanade, "An iterative image registration technique with an application to stereo vision," in *Proceedings of the 7th International Joint Conference on Artificial Intelligence - Volume 2*, ser. IJCAI'81. San Francisco, CA, USA: Morgan Kaufmann Publishers Inc., 1981, pp. 674–679.

[8] S. Baker and I. Matthews, "Lucas-kanade 20 years on: A unifying framework." *International Journal of Computer Vision*, vol. 56, no. 3, pp. 221 – 255, 2004.

[9] E. Antonakos, J. Alabort-i Medina, G. Tzimiropoulos, and S. Zafeiriou, "Feature-based lucas-kanade and active appearance models," *Image Processing, IEEE Transactions on*, vol. 24, no. 9, pp. 2617–2632, Sept 2015.